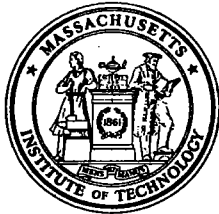


WHOI-83-18

*Copy 1*

WOODS HOLE OCEANOGRAPHIC INSTITUTION/  
MASSACHUSETTS INSTITUTE OF TECHNOLOGY



1930

JOINT  
PROGRAM  
IN  
OCEANOGRAPHY  
AND  
OCEAN ENGINEERING

WHOI  
DOCUMENT  
COLLECTION

DOCTORAL DISSERTATION

FLOW AND SKIN FRICTION

OVER NATURAL ROUGH BEDS

BY

CHRISTOPHER PAOLA

JUNE 1983

WHOI-83-18

FLOW AND SKIN FRICTION OVER NATURAL ROUGH BEDS

By

Christopher Paola



WOODS HOLE OCEANOGRAPHIC INSTITUTION  
Woods Hole , Massachusetts 02543

June 1983

DOCTORAL DISSERTATION

*Funding was provided by the National Science Foundation under Grant OCE 77-20437 and by the Office of Naval Research under Contract N00014-80-C-0273.*

*Reproduction in whole or in part is permitted for any purpose of the United States Government. This thesis should be cited as: Christopher Paola, 1983. Flow and Friction Over Natural Rough Beds. Sc.D. Thesis. Massachusetts Institute of Technology/Woods Hole Oceanographic Institution WHOI-83-18.*

*Approved for public release; distribution unlimited.*

Approved for Distribution:

*R. P. Von Herzen*

Richard P. von Herzen, Chairman

*Charles D. Hollister*

Charles D. Hollister  
Dean of Graduate Studies



FLOW AND SKIN FRICTION OVER NATURAL ROUGH BEDS

by

Christopher Paola

B.S., Lehigh University (1976)

M.Sc., University of Reading (1977)

Submitted to the Department of Earth and Planetary Sciences,  
Massachusetts Institute of Technology, and to the Department  
of Geology and Geophysics, Woods Hole Oceanographic  
Institution, on February 16, 1983, in partial fulfillment of  
the requirements for the Degree of

DOCTOR OF SCIENCE

at the

MASSACHUSETTS INSTITUTE OF TECHNOLOGY

and the

WOODS HOLE OCEANOGRAPHIC INSTITUTION

February, 1983

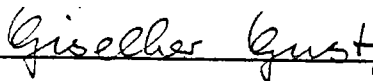
© Massachusetts Institute of Technology 1983

Signature of Author:



Joint Program in Oceanography,  
Massachusetts Institute of Technology and  
Woods Hole Oceanographic Institution

Certified by:



Thesis Supervisor

Certified by:



Thesis Supervisor

Accepted by:



Chairman, Joint Committee for Marine  
Geology and Geophysics



# FLOW AND SKIN FRICTION OVER NATURAL ROUGH BEDS

by

Christopher Paola

Submitted to the Department of Earth and Planetary Sciences, Massachusetts Institute of Technology, and to the Department of Geology and Geophysics, Woods Hole Oceanographic Institution, on February 16, 1983, in partial fulfillment of the requirements for the Degree of Doctor of Science in Oceanography

## ABSTRACT

When a boundary layer develops over a bed that is hydrodynamically rough at a length scale or scales larger than the grain size (a macrorough bed), as is usually the case where bed forms are present, it is necessary to distinguish among total boundary shear stress and its components, form drag and spatially averaged skin friction. It is known that the mean-velocity field reflects the composite boundary shear stress. Above about one roughness height above the tops of the roughness elements, the velocity does not vary horizontally. Its vertical profile is semilogarithmic and scales with the total friction velocity  $u_*^t$  and total roughness length  $z_{ot}$ . This region is here called the integrated logarithmic layer (ILL). Below the ILL the velocity varies horizontally in response to the irregular boundary; this region is called the surface layer.

In the first of two sets of experiments reported here, skin-friction measurements were made with an array of flush-mounted hot films at four points on the stoss slope of one of a field of two-dimensional immobile current ripples. Total boundary shear stress was also measured, as were mean-velocity profiles in the ILL and the surface layer. The ILL behaves as described above. Although surface-layer velocity profiles are semilogarithmic, their semilogarithmic slope is not proportional to the local skin-friction velocity, so they do not locally obey the law of the wall. Rather, the velocity field can be decomposed into a spatially averaged rotational component and a local inviscid perturbation. The measured skin-friction field is consistent

with a simple model for sediment transport over the bed forms except near reattachment, where the fluctuating skin friction is important. The data are also consistent with the drag-partition theories of Einstein and Barbarossa (1952) and Engelund (1966). Normalized skin-friction spectra do not vary with streamwise position but do vary with Reynolds number; skin-friction probability density functions show significant increases in skewness and kurtosis near reattachment but do not vary strongly with Reynolds number.

In the second set of experiments the skin-friction vector field was measured around isolated hemispheres, with model sedimentary tails one and four obstacle heights long and without tails. The measured skin-friction fields are not consistent with deposition along the obstacle-flow centerline downstream of reattachment, which occurs about two obstacle heights downstream of the trailing edge of the hemisphere. This applies for local bed-load erosion and deposition and for general deflation of the bed, and is not substantially altered by the presence of either tail. Measurements were also made of skin friction, total boundary shear stress and ILL velocity profiles over  $h, B$ -rough arrays of hemispheres with and without tails four roughness heights long, at two areal densities. The skin-friction field in the denser array is significantly distorted from that around an isolated element. The measured skin friction in both arrays is significantly greater than that given by a drag-partition formula proposed by Wooding et al. (1973). The roughness length  $z_{ot}$  for both densities is not changed by addition of the tails.

Thesis supervisors: Dr. John B. Southard

Title: Associate Professor of Earth and Planetary  
Sciences

Dr. Giselher Gust

Title: Associate Professor of Marine Science,  
University of South Florida

## ACKNOWLEDGEMENTS

It is a pleasure to thank Giselher Gust and John Southard for the guidance they have given me over the past five years. The science described in this dissertation falls in the common ground between fluid physics and sedimentary geology. Although both GG and JS are strongly interdisciplinary scientists, each has contributed to my education and to this work from his own perspective; broadly, GG from physics and JS from sedimentology. I am grateful to them both for their willingness to cooperate, without which this dissertation could not even have been begun.

I thank Giselher Gust for providing most of the direct supervision of the work described here, for patiently teaching me a great deal about physical and experimental science, and for generously providing much of the equipment and technical support necessary for the completion of the experiments. All the digital data processing was done at his laboratory at the University of South Florida, much of it by B. Allen Patrick, for whose enthusiasm, skill, and generous hospitality I am extremely grateful.

I thank John Southard for his guidance and advice during my graduate career, and particularly for providing a stimulating research environment in which I was exposed to a wide range of problems related to physical sedimentology. I have learned a great deal from him, both directly and by example. Much of whatever clarity of expression this dissertation possesses reflects his influence.

I am grateful to Bill Grant, Mark Wimbush, and Charley Hollister, all members of my thesis committee, for careful and constructive readings of the manuscript, and to Dave Johnson for chairing the defense. In addition, I thank them all for many enlightening discussions during my time in the Joint Program. I particularly wish to thank Dave Johnson for helping me find my way, and Yogi Agrawal for generously sharing home and insight over the past two years.

I thank Donna Hall for carefully drafting many of the figures, John Annese for technical help generously given at several stages of the work, and Judith Stein for deftly untangling our project's allotment of red tape.

My graduate career has been enhanced considerably by lively and diverse discussions with my fellow students. In particular, I thank Kevin Bohacs and Bill Corea for helping me get started; Roger Kuhnle and Peter Vrolijk, who worked with me on the experiments, for their enthusiasm and ingenuity; Steve and Ann Swift for their patience and kind hospitality; Doug Walker, for his superb "get-it-donedness";



and Peter Wilcock for his good-natured insight and uncommon sense. I thank them all for their friendship and for sharing their understanding with me.

I thank Kathy, Hope, Mark, Jim, and Mary Lee for their love and support, particularly during the past year.

I thank Barb Russell for her love and support throughout the most difficult stages of my graduate career.

Finally, there is a debt of gratitude that I wish to record but can never repay; it is to my family. My father Nicholas, my mother Mary, and my sister Suzanne have helped me more than they can ever know. The name on the title page is also theirs, and if the work within is worthy of that I will be well satisfied. This dissertation is dedicated to them.

Financial support. I received fellowship support from the National Science Foundation for three years, and early stages of this project were supported by NSF grant OCE 77-20437. Most of the work was done under Office of Naval Research contract number N00014-80-C-0273.

Contents	Page
Acknowledgements.....	4
List of Figures.....	9
List of Tables.....	14
Chapter 1. Introduction.....	15
1.1. General.....	15
1.2. Experimental methods.....	36
1.21. General.....	36
1.22. The flume.....	36
1.23. Thermal anemometry.....	40
1.24. Data processing.....	54
Chapter 2. Flow and skin friction over two-dimensional current ripples.....	59
2.1. Introduction.....	59
2.11. Internal boundary layers.....	62
2.12. Application of IBL theory to flow over macrorough beds.....	66
2.2. Experimental methods.....	78
2.3. Results: mean quantities.....	95
2.31. Skin friction.....	95
2.32. Velocity.....	99
2.4. Results: fluctuating quantities.....	123
2.41. Root-mean-square intensity.....	123
2.42. Spectra.....	133
2.43. Probability density functions.....	144
2.5. Discussion.....	155
2.51. Why is the local response inviscid?.....	155

	Page
2.52. Comparison of the results with drag-partition theories.....	166
2.53. Application to sediment-transport calculations.....	171
2.54. Implications for bed-form dynamics and classification.....	178
2.6. Conclusions.....	187
Chapter 3. Flow and skin friction over three-dimensional macrorough beds.....	189
3.1. Introduction.....	189
3.2. Experimental methods.....	206
3.3. Results: isolated elements.....	238
3.31. Direction.....	238
3.32. Mean skin-friction magnitude.....	245
3.33. RMS skin friction.....	257
3.34. Horizontal divergence.....	268
3.4. Results: full fields.....	280
3.41. Skin friction.....	280
3.42. Velocity profiles.....	286
3.5. Discussion.....	298
3.51. Obstacle-trapped bed forms.....	298
3.52. Skin-friction patterns in relation to overall flow resistance.....	305
3.53. Application of the full-field results to natural conditions.....	308
3.6. Conclusions.....	323

	Page
4. References.....	325
Appendix A. Symbols.....	334
Appendix B. Computer programs.....	339
Biographical sketch.....	347

## List of Figures:

Figure		Page
1.1	Sketches of smooth, rough, and macrorough flows	19
1.2	General Cartesian coordinate system (x,y,z) and corresponding velocity components (u,v,w).	21
1.3	General features of a bed form and its associated flow field.	31
1.4	The flume in which all the experiments were done.	37
1.5	Schematic section of flow and the thermal boundary layer about a hot wire.	41
1.6	Simplified diagram of the circuitry for a constant-temperature thermal anemometer.	45
1.7	Schematic diagram of flow and the thermal boundary layer over a flush-mounted hot film.	50
1.8	The instrument chain used for recording digital data.	55
2.1	Simplified diagram of an internal boundary layer developing at a smooth-to-rough transition ( $z_{o2} > z_{o1}$ ).	63
2.2	An internal boundary layer model for the velocity field over bed forms of large aspect ratio ( $O(100)$ ), after Smith and McLean (1977).	69
2.3	The idealized two-part semilogarithmic form of the spatially averaged mean-velocity profile in macrorough flows possessing an equilibrium sublayer.	73
2.4	The TSI hot-wire sensor used to measure velocity in the two-dimensional ripple experiment.	81
2.5	Hot-wire calibration curves for each of the three runs in which velocity measurements were made.	83
2.6	(A) Photograph and (B) section of the hot-film array used to measure skin friction in the two-dimensional ripple experiment.	87

Figure	Page
2.7	Calibration curves for the skin-friction array shown in figure 2.6. 90
2.8	Comparison of the output voltage of a hot film mounted on a rubber substrate that is flat (squares) and curved normal to the direction of flow (circles) for different values of flow speed given in arbitrary units (the range of speeds is about 3 - 40 cm/s). 93
2.9	Mean values measured with the skin-friction array shown in figure 2.6, nondimensionalized with $u_*\tau$ , as a function of $R_*$ and sensor position. 97
2.10	Sketch of the curvilinear vertical coordinate $\zeta$ in comparison with the rectilinear coordinate $y$ . 101
2.11	Mean-velocity profiles measured over two-dimensional ripples, nondimensionalized with the total friction velocity $u_*\tau$ . 103
2.12	Mean-velocity profiles measured over two-dimensional ripples, nondimensionalized with the local skin-friction velocity $u_*s$ , for skin-friction measuring positions 1 (A), 2 (B) and 3 (C). 107
2.13	Sketch of the velocity field given by first-order potential theory for flow over a sinusoidal bed. 115
2.14	Measured dimensional velocity profiles (open symbols) compared with the results (filled symbols) of adding a first-order inviscid solution to the profile measured at position 2. 119
2.15	The rms value $\sigma_\tau$ of the fluctuating skin friction as a function of $R_*$ and sensor position, in dimensional form (dynes/cm <sup>2</sup> ) and nondimensionalized with the total bottom stress $\tau_{ot}$ . 125
2.16	Relative fluctuation intensity $\sigma_\tau/\tau_{os}$ of skin friction measured over two-dimensional ripples as a function of sensor position and $R_*$ . 128
2.17	Relative fluctuation intensity $\sigma_\tau/\tau_{os}$ of skin friction as a function of bulk Reynolds number $Du/\nu$ for smooth flow. 130

Figure	Page	
2.18	Power spectral density $\phi$ of the skin friction, normalized by the total variance of the signal $\sigma_{\tau}^2$ , as a function of frequency $f$ . The data shown were measured at the crest (1) and near reattachment (3).	135
2.19	Nondimensional skin-friction spectra measured on two-dimensional ripples and in smooth flow.	141
2.20	Skin-friction probability density functions for all sensor positions and roughness Reynolds numbers.	145
2.21	Mean-velocity profiles measured by Zilker (1976) at different streamwise positions over a sinusoidal bed (open symbols) compared with the results (filled symbols) of adding a first-order inviscid solution to the profile measured at $x/L = 0.8$ .	161
2.22	Profiles of Reynolds shear stress obtained by Zilker (1976) at different streamwise positions over a sinusoidal bed.	163
2.23	Calculated skin-friction-velocity profiles (heavy lines) required to maintain a stable propagating ripple form, compared with measured values (open circles), for two values of $R^*$ .	175
2.24	The surface-layer velocity profile over a bed form of small ( $O(10)$ ) aspect ratio viewed as the sum of a spatially averaged rotational profile and a local irrotational perturbation.	181
3.1	Sketch of the "horseshoe" vortex system about a cylindrical obstacle on a flat bed.	195
3.2	The three roughness elements around which skin-friction measurements were made in the first (isolated-element) series of runs.	209
3.3	One of the flush-mounted hot-film sensors used in the first series of runs, together with the grid used to position the roughness elements.	211
3.4	Locations where the skin-friction field was measured in the first series of runs.	213

Figure		Page
3.5	Calibration curves for single flush-mounted hot films used in the first series of runs.	215
3.6	(A) Photograph and (B) plan of the sensor array used to gather skin-friction data in the second (full-field) series of runs.	217
3.7	Calibration curves for the seven skin-friction sensors of the array shown in figure 3.6.	220
3.8	The metal-clad hot-wire sensor used to measure velocity in the second (full-field) series of runs.	223
3.9	The calibration curve for the velocity sensor shown in figure 3.8.	227
3.10	Plan view of roughness unit cells for the (A) sparse and (B) dense arrays used in the full-field runs.	231
3.11	Mean-velocity profiles measured over the sparse ( $\lambda = 0.00845$ ) array of hemispheres at the two positions shown in figure 3.10.	233
3.12	(A) and (B) Photographs of a plaster plate showing the direction field behind an isolated hemisphere.	239
3.13	Direction fields behind isolated obstacles, determined from plaster plates like that shown in figure 3.12.	241
3.14	The skin-friction magnitude field interpolated from measurements behind isolated obstacles at the points shown in figure 3.4, nondimensionalized by the reference (free-stream) value.	247
3.15	The root-mean-square skin-friction field interpolated from measurements behind isolated obstacles at the points shown in figure 3.4, nondimensionalized by the reference (free-stream) skin friction.	258
3.16	The horizontal divergence of the time-averaged skin-friction field.	270
3.17	Mean-velocity profiles measured in the four full-field runs.	287



Figure		Page
3.18	Mean-velocity profiles for the four full-field runs nondimensionalized according to the scheme of Wooding <u>et al.</u> (1973).	293
3.19	Mean-velocity profiles for the four full-field runs, nondimensionalized as in figure 3.18 but excluding the factor $\phi$ introduced by Wooding <u>et al.</u> (1973) to account for the effect of the streamwise extent of roughness elements on the roughness length $z_{ot}$ .	295
3.20	Sketches of the vortex system behind an isolated hemisphere (A) with no stratification and (B) with stable stratification.	303
3.21	The two-dimensional region of influence for a measuring station S in a boundary-layer profile.	313
3.22	Roughness-averaging scales for a series of regions upstream of a hypothetical boundary-layer measuring station (circle), based on the data in Table 3.5.	317

## List of Tables

Table	Page
2.1 General experimental conditions for runs over two-dimensional current ripples	79
2.2 Skin-friction skewness as a function of sensor position and roughness and bulk Reynolds numbers	152
2.3 Skin-friction kurtosis as a function of sensor position and roughness and bulk Reynolds numbers	153
2.4 Skin-friction skewness and kurtosis measured in smooth flow	154
2.5 Comparison of nondimensional spatially averaged skin-friction velocities calculated according to the method of Einstein and Barbarossa (1952) with values measured in this study	168
2.6 Comparison of Engelund's (1966) method for calculating form drag with the results of this study	170
3.1 Correspondence between calibrations shown in figure 3.5, correlation coefficients for fitted power-law curves, and chronological run numbers for the first (isolated-element) series of runs	225
3.2 Experimental conditions for runs of the first (isolated-element) series	244
3.3 Experimental conditions for runs of the second (full-field) series	281
3.4 Time-averaged skin-friction magnitude at the seven positions shown in figure 3.6	283
3.5 The limits of the upstream region that influences each height in a hypothetical current-meter array, and the roughness averaging scale $L_r$ in each region, for a typical $z_{ot}$ of 0.1 cm	322

## 1. Introduction.

1.1. General. Much of physical sedimentology involves consideration of the motion of fluid and sediment over boundaries irregular on one or more scales. Bed forms are among the commonest sources of irregularity, and they are of particular importance geologically because in many cases they produce a sedimentary record that is distinctive and potentially rich in paleoenvironmental information. In the analysis of modern environments, bed forms play an important role as natural current meters; the information they provide is potentially most valuable in places such as the deep ocean where direct measurement of currents is difficult and expensive. Interpreting both the ancient and the modern bed-form records amounts to deducing flow properties from observations of bed-form characteristics. This may be viewed as an inverse problem in which the forward problem is to determine the properties of bed forms developed under a given imposed flow field. This forward problem in itself is extremely complex: the simplest elements to which it can be reduced form a coupled, turbulent system of flow and sediment transport under locally nonuniform conditions. In the face of this it is not surprising that the most productive approach from a sedimentological viewpoint has been direct and empirical (Southard, 1971; Dalrymple et al., 1978; Harms et al., 1982).

As in any branch of science, however, such empirical information must always be supplemented by analysis aimed at providing an understanding of why the results have the form they do. Apart from the aesthetic pleasure such understanding provides, without it we cannot assess the stability of empirical results to changes in conditions from those under which they were obtained. Spatial and temporal variations in scale and magnitude of flow and in sediment properties all affect bed forms in nature; to evaluate the effects of all of these empirically we would have to generate an enormous catalog of data. A more effective approach is one that combines theory with well-placed critical experiments.

So much for putting the general problem of bed-form dynamics into geological perspective; it still needs to be reduced substantially to bring it within range of the available means of attack. I mentioned above that any bed-form theory must involve consideration of both flow and sediment transport over irregular (henceforth "rough") boundaries. I have chosen to concentrate on the flow, because the flow field must be understood at least near the boundary before there is any hope of calculating the sediment transport. There are, however, complex problems relating to the sediment transport as well. Some of them will be discussed in section 2.53, but the main emphasis in this work will be on the flow and the tangential bottom stresses it sets up.

The nature of the boundary shear stress depends on the form of the boundary, as illustrated by the three cases shown in figure 1.1. In all three, it is assumed that the boundary layer is steady, uniform, and unstratified, and that no sediment transport is occurring. ("Boundary layer" will usually be used in a general sense to mean that part of a wall-bounded shear flow in which shear stresses generated near the wall are dynamically important. Occasionally, though, it will be necessary to distinguish among pipe, open-channel and developing boundary layers.) More detailed discussion of most of the following review can be found in Tennekes and Lumley (1972, ch. 5), Arya (1975), Townsend (1976, ch. 5), and Smith and McLean (1977).

Consider first a turbulent boundary layer developed over a perfectly smooth surface (figure 1.1a). (We will see presently that many real surfaces are "smooth enough".) Although the boundary layer is fully turbulent, as we approach the wall the viscosity must become important to satisfy the no-slip condition. Hence the flow near the wall is viscous-dominated; at the wall the Reynolds stress is extinguished and the instantaneous boundary shear stress  $T_0$  is given by  $T_0 = \rho \nu (\partial U / \partial y)_0$ , where  $\rho$  and  $\nu$  are the fluid density and kinematic viscosity respectively, and  $U$  is the instantaneous velocity at height  $y$  above the bottom (figure 1.2). The subscript zero indicates that both the stress and the vertical derivative are to be evaluated at the bed.

In a turbulent flow  $T_0$  and  $U$  can be divided into time-averaged and fluctuating parts. Nearly all of the flows to be considered in this work will be turbulent; variables describing them will be distinguished as follows. All literal references will be to time-averaged quantities unless stated otherwise. Among symbolic references, lower-case letters or overlining will denote time-averaged quantities, primed lower-case letters will denote temporal fluctuations, and upper-case letters will denote total instantaneous quantities. Thus  $A = \bar{a} + a'$  where  $\bar{a} = (1/t_a) \int_0^{t_a} A dt$ , and  $t_a$  is a time scale long compared with those of the turbulent fluctuations.

Anticipating that  $\tau_0$  as well as  $\nu$  may influence the flow field near the smooth wall, we define a kinematic mean shear stress  $u_* = (\tau_0/\rho)^{1/2}$  having units of velocity and called the friction velocity or shear velocity. Then a natural length scale is  $\nu/u_*$  and the velocity field near the bed is given by

$$\frac{u}{u_*} = f_s\left(\frac{u_* y}{\nu}\right) \quad 1.1$$

Far from the wall, in the outer part of the flow, the turbulence begins to be affected by the finite height of the boundary layer  $D$ , so  $D$  becomes the length scale. Since the outer scaling is to be viewed as being applied from the surface downward, we refer the velocity to the surface velocity  $u_s$ ; it should also scale with  $u_*$ , on the grounds that whatever is the overall driving force on the flow

Figure 1.1. Sketches of smooth, rough, and macrorough flows (left) and corresponding mean-velocity profiles (right). Multivalued profiles are for different streamwise positions.

VDL - Velocity-defect layer

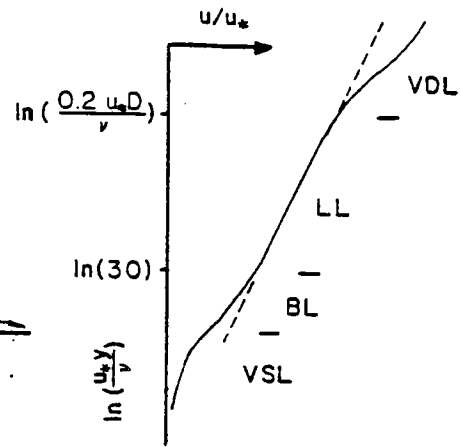
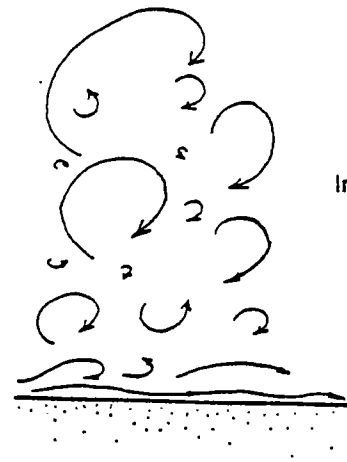
LL - Logarithmic layer

BL - Buffer layer

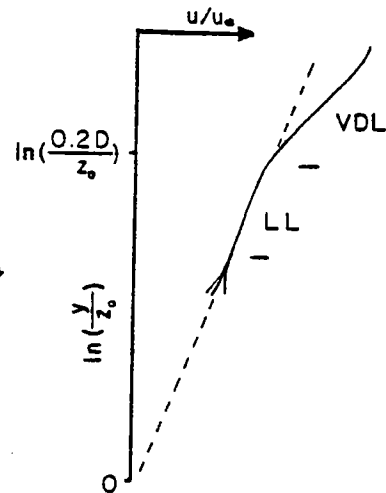
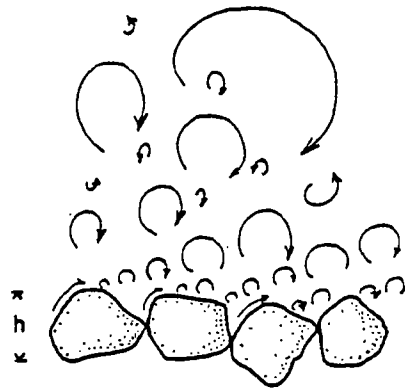
VSL - Viscous sublayer

ILL - Integrated logarithmic layer

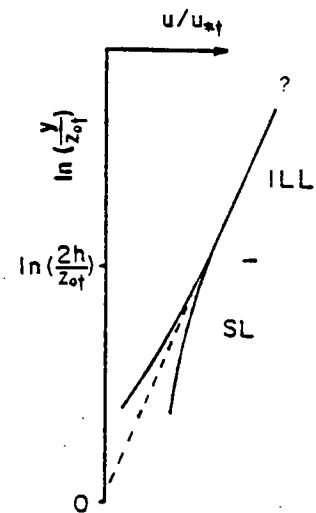
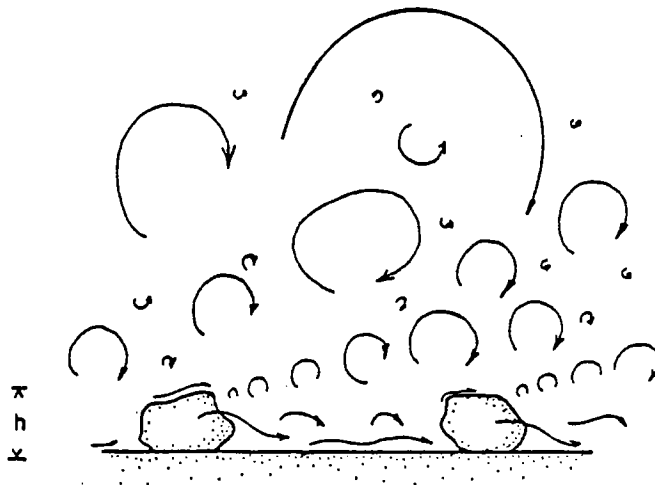
SL - Surface layer



A. SMOOTH



B. ROUGH



C. MACROROUGH



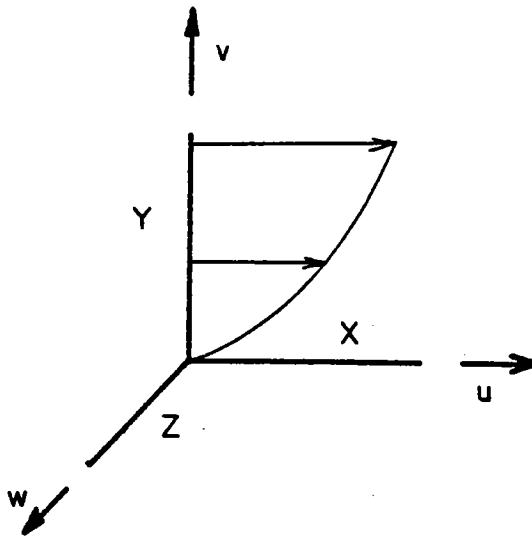


Figure 1.2. General Cartesian coordinate system  $(x, y, z)$   
and corresponding velocity components  $(u, v, w)$ .

(usually gravity or pressure), it must be balanced by the boundary shear stress. Hence for the outer layer

$$\frac{u_s - u}{u_*} = g \left( \frac{y}{D} \right) \quad 1.2$$

Millikan (1939) showed that by requiring that both (1.1) and (1.2) hold in some "overlap region" the velocity profile there is specified to within two empirical constants:

$$\frac{u}{u_*} = a_1 \ln \left( \frac{u_* y}{\nu} \right) + a_2 \quad 1.3$$

This relation was originally derived in a different way, so to maintain consistency  $a_1$  is usually written as  $1/\kappa$  where  $\kappa$  is called the von Karman constant. Much has been written about the constancy of  $\kappa$ ; it certainly has the value 0.4 in smooth flow for the three general types of boundary layer named above over the range of Reynolds numbers attainable in the laboratory. This makes (1.3) a very powerful tool: it is relatively difficult to measure  $u_*$  directly, particularly in field experiments, but it can be determined from (1.3) as  $u_* = \kappa du/d(\ln(y))$ . Making the required velocity-profile measurements is usually relatively straightforward.

The numerical value of  $a_2$  is of less interest for our purposes. It is similarly constant at about 5.0.

So for a smooth turbulent boundary layer the velocity profile looks as shown in figure 1.1a. Immediately above the bed there is a viscous-dominated region called the viscous sublayer in which the profile is linear:  $(u/u_*) = (u_* y / \nu)$ . This is overlain by a buffer or transitional region and then

the logarithmic layer; the velocity profile there is often loosely referred to as the "law of the wall" although strictly speaking this governs the two layers below as well. Beyond this is the outer or "velocity-defect" region, governed by a form of (1.2) that varies according to whether the boundary layer is fully developed in a pipe or in an open channel, or is not fully developed.

Now consider a turbulent boundary layer over a uniform bed of coarse sand of diameter  $h$  (figure 1.1b). By analogy with flow about an isolated sphere one would expect that, if velocities near the bed are large enough, flow separation should occur around the grains and the resulting wakes should disrupt the velocity field. We define a roughness Reynolds number  $R^* \equiv u_* h / \nu$ ; empirically, if  $R^*$  is greater than about 5, the viscous sublayer is affected by the presence of the grains, and if  $R^*$  is greater than about 70 (fully rough flow) it is completely destroyed in a formal sense. Of course, there must still be a viscous-dominated region on the surface of each grain to satisfy the no-slip condition, and with it a viscous shear stress. Continuing our analogy with the behavior of an isolated sphere, however, we expect the dominant part of the drag on the grains to be pressure or form drag induced by the separated flow about the grains. The boundary shear stress, in which this drag is averaged over the bed, is thus independent of viscosity and so of  $R^*$ .

The scaling arguments outlined for smooth flow can be extended to the fully rough case, provided we exclude from consideration the region very near the bed where the grains affect the flow field individually (figure 1.1b). The length scale in the law of the wall includes the viscosity, which is clearly inappropriate here; it is natural instead to choose  $h$ , the grain height, as the inner length scale. We retain  $u_*$  as the scaling velocity and write the law of the wall as

$$\frac{u}{u_*} = f_r\left(\frac{Y}{h}\right) \quad 1.4$$

The outer flow, on the other hand, includes no explicit dependence on  $\nu$  so there is no reason to modify (1.2) for rough flows. In an overlap region where (1.4) and (1.2) are both valid, we obtain the rough-bed equivalent to (1.3):

$$\frac{u}{u_*} = a_3 \ln\left(\frac{Y}{h}\right) + a_4 \quad 1.5$$

It is one of the most fundamental and remarkable results of the study of turbulent boundary layers that  $a_3 = a_1$ ; that is, that the relation between  $u_*$  and  $du/d(\ln(y))$  in the logarithmic region is the same in both smooth and rough flows. On the other hand,  $a_4$  is different from the smooth case and depends on the geometry of the roughness. It is usual to rewrite (1.5) as

$$\frac{u}{u_*} = \frac{1}{\kappa} \ln\left(\frac{Y}{z_0}\right) \quad 1.6$$

where  $z_0$  is called the roughness length; it is a length scale proportional to the scale of the roughness. The constant of proportionality depends on the roughness geometry. (Here I

am generalizing slightly from the example of closely packed sand under consideration to similar kinds of small-scale, uniformly distributed roughness.) For closely packed sand-grain roughness,  $z_o=h/30$ .

It is possible to imagine sediment transport under either smooth or rough conditions as described above, although for the smooth case the viscous sublayer is disrupted by the moving grains (Gust and Southard, in press) and the length scale in  $R^*$  may need to be redefined. In any case the force propelling the sediment is the boundary shear stress  $\rho u_*^2$ : for both kinds of boundary layer considered so far, this is the average tangential force per unit area on the grains.

Now suppose we have a similar situation -- a bed roughened with large (say a few centimeters), closely packed spherical grains -- but imagine them to be laid in a single layer on a flat, smooth surface. Water flows over the bed so that  $u_*$  is about 1 cm/s and  $R^*$  is a few hundred, comfortably above the limit for fully rough flow. What happens if we remove grains one at a time, leaving individual grains surrounded by smooth surface (figure 1.1c)? (It would be necessary to adjust the mean velocity continuously to keep the boundary shear stress constant.) The large grains still separate the flow, exert form resistance, and shed wakes that locally disrupt the viscous sublayer. But the no-slip condition implies the existence of a viscous-dominated region near the wall: at the bed surface the boundary shear stress has the same

viscous form as it does on a smooth wall:  $\tau_o = \rho v (\partial u_p / \partial y_n)_o$ , where  $y_n$  is locally normal to the bed and has its origin at the bed surface, and  $u_p$  is the velocity locally parallel to the surface. Such small-scale, local shear stress is known as skin friction. Due to gradients in pressure and turbulence intensity induced by the presence of the large grains, the skin friction varies with position over the bed.

We may define the total bottom stress  $\tau_{ot}$  as

$$\tau_{ot} = \frac{1}{A} \left( \int_{A'} p_o n_y dA' + \int_{A'} \rho v \left( \frac{\partial u_p}{\partial y_n} \right) n_y dA' \right) \quad 1.7$$

where  $A$  is an averaging area that includes a number of roughness elements,  $A'$  is a true wetted surface area,  $p_o$  is the local pressure on the boundary,  $n_y$  is the vertical component of a unit vector normal to the surface, and  $u_p$  is the velocity parallel to the surface. This is the total boundary shear stress acting against the flow, so that in a wide, uniform open channel of depth  $D$  and slope  $S$ ,

$$\tau_{ot} = \rho g D S \quad 1.8$$

The first term in (1.7) is called the form drag ( $\tau_{of}$ ); it is meaningful only in a spatially averaged sense. On the other hand, the skin friction ( $\tau_{os}$ ) is the integrand in the second term; it is a well-defined local quantity although it enters the total bottom stress in spatially integrated form.

The boundary layer over a bed of widely and perhaps irregularly spaced roughness elements is thus considerably more complicated than either a rough or a smooth boundary layer; it really combines elements of both. The work to be

described in this thesis is aimed at clarifying aspects of this type of flow, which will be referred to as macrorough. Most of the further discussion of macrorough flow will be left to later, more detailed sections, but a few additional general comments should be made here. First, each of the three boundary shear stresses in (1.7) --  $\tau_{ot}$ ,  $\tau_{of}$ , and  $\tau_{os}$  -- can be converted to a friction velocity  $u_* = (\tau_o)^{1/2}$ . In light of the role of  $u_*$  in scaling velocity profiles, embodied in (1.2), (1.3) and (1.6), one would expect the composite nature of the boundary shear stress to be reflected in the velocity field. We can get a rough idea of how this works by considering the consequences of a general increase in the length scale of the turbulence with height, which in turn is a simple kinematic result of the increasing distance of the eddy centers from the wall (Townsend, 1976, p. 156 ff.). As eddies become larger, they respond more slowly to changes in strain rate, and as their distances from the wall increase, they are advected more quickly by the mean velocity; the net result of both effects is that the area of the bed to which the turbulence responds increases with height in the flow (Townsend, 1965a). (These ideas will be developed in more detail in section 3.53.) Since the total bottom stress  $\tau_{ot}$  is spatially averaged by definition (1.7), it can be a valid scaling parameter only above some height at which the turbulence is large enough to average the variable bottom stress. This height cannot be less than some small

distance above the tops of the roughness elements (empirically, it will be seen in section 2.32 to be about one roughness height), because the form drag, included in (1.7) as an integral of pressure on the boundary, appears in the flow as excess Reynolds stress generated in the wakes of the roughness elements. One must be somewhere above the tops of the roughness elements before the wakes will have merged to produce a Reynolds-stress field that is uniform in the streamwise direction. Below this, the velocity and turbulence fields vary spatially in response to the rough topography.

Combining all of the above, the following picture emerges. In macrorough flow, the spatially integrated region well above the tops of the roughness elements corresponds to the logarithmic layer given by (1.6); it will be referred to here as the integrated logarithmic layer (ILL). In deriving the profile law (1.6) for fully rough flow, a single friction velocity equivalent to  $u_*^t$  emerged naturally as the velocity scale because there was no need to consider the details of the viscous shear stress on the grain surfaces. But in macrorough flow there are areas between roughness elements where the boundary shear stress is purely viscous; furthermore the disposition of this viscous stress and its contribution to the total boundary shear stress both depend on the geometry and arrangement of the roughness elements.



